Applied Surface Science 261 (2012) 268 -275 doi: 10.1016/j.apsusc.2012.07.159

Study of ZnO:Al films for silicon thin film solar cells

H. Zhu[1, *], J. Hüpkes[1], E. Bunte[1], S. M. Huang[2]

[1]IEK5-Photovoltaik, Forschungszentrum Jülich GmbH, D-52425 Jülich, Germany

[2]Engineering Research Center for Nanophotonics and Advanced Instrument, Ministry of Education, East China Normal University, 200062, Shanghai, P. R. China

[*] Corresponding author. Email: hongbing1982@hotmail.com

Abstract

In this study, aluminum doped zinc oxide (ZnO:Al) films deposited from dual rotatable ceramic targets are systematically investigated. The influences of substrate temperature and working pressure as well as discharge power on different properties of ZnO:Al films including deposition rate, surface structure, optical and electrical properties as well as etching behaviors are studied. It is found that in addition to substrate temperature and working pressure the discharge power plays an important role in material properties of ZnO:Al films. Low rate ZnO:Al (LR-AZO) films with high carrier mobility of about 50 Vs/cm^2 and high rate ZnO:Al (HR-AZO) films of more than 90 nm·m/min with high carrier mobility of about 45 Vs/cm^2 are achieved. However, there is only a narrow parameter window to achieve a regulated crater-shape surface structure for ZnO:Al films after a chemical wet etching process. The surface-textured ZnO:Al films were applied in silicon thin film solar cells and high efficiencies of 8.5% and 11.3% are achieved for single junction hydrogenated microcrystalline silicon (μc-Si:H) solar cells and amorphous/ microcrystalline silicon (a-Si:H /μc-Si:H) tandem solar cell, respectively.

Key words: ZnO:Al thin films, Magnetron sputtering, Chemical wet etching, Rotatable target

0. Introduction

Surface-textured transparent conductive oxide (TCO) films are usually applied in silicon thin film solar cells as front contact to enhance the short circuit current (J_{sc}) and conversion efficiency due to their good light scattering effect [1, 2]. Surface-textured aluminum doped zinc oxide (ZnO:Al) film is an important TCO material for such an application [1]. ZnO:Al films prepared by magnetron sputtering are usually chemically etched in diluted HCl solution to achieve a rough surface structure [1, 3-6]. An optimum surface structure i.e. crater-shape of sputtered ZnO:Al films after etching strongly depends on specific deposition conditions [7]. Kluth et al. [7] reported three types of surface structures based on modified Thornton model, which strongly depend on substrate temperature and working pressure. Besides, Berginski et al. [8, 9] studied the role of the target aluminum concentration (TAC) on the optimization of surface textured ZnO:Al films for the application in silicon thin film solar cells. They found the optimized surface structure (Type II) of films with a low TAC should require relatively high substrate temperatures. In addition, the oxygen partial pressure would lead to different material properties [10, 11]. As a matter of fact, other deposition conditions like discharge power would also affect etching behaviors and surface structures as well as optical and electrical properties of ZnO:Al films. Thus, the systematical study on the influences of the main deposition conditions i.e. discharge power, substrate temperature and working pressure on ZnO:Al films would be much significant for the further optimizations of material properties and corresponding silicon thin film solar cell performances.

In this study, the ZnO:Al films were prepared from dual rotatable ceramic targets. The influences of substrate temperature and working pressure as well as discharge power on various properties of ZnO:Al films including deposition rate, surface structure, optical and electrical properties as well as etching behaviors are systematically investigated. Finally, surface-textured ZnO:Al films were applied in silicon thin film solar cells to check their application functions.

1. Experimental details

ZnO:Al films were prepared on Corning glass substrates (Corning, Eagle XG) in an in-line sputtering system (VISS 300 by Von Ardenne Anlagentechnik, Dresden, Germany). Rotatable dual

magnetrons (RDM) with ZnO:Al_2O_3 (99.5:0.5 wt%) ceramic tube targets (760 mm in length) were mounted in the deposition chamber. The schematic of sputtering system with dual rotatable ceramic targets is shown in **Fig. 1.** The sputtering deposition was operated under mid-frequency (MF) excitation at 40 kHz. The substrate temperature varied between 225ºC and 350ºC. The applied discharge power was between 2 kW and 14 kW in total and the working pressure varied from 0.5 Pa to 2.0 Pa. The texturing of the as-deposited flat ZnO films was carried out by wet chemical etching in diluted hydrochloric (HCl) acid solution (0.5 wt%) at room temperature (21°C). A novel two-step etching method, of which first etching step is carried out in diluted HF solution (1%) for a few seconds and then followed by the second etching in diluted HCl solution (0.5%) for more durations, was developed for ZnO:Al films to improve the surface structures. Surface-textured ZnO films, as served as front contact electrodes, were applied in single junction p-i-n hydrogenated microcrystalline silicon (μc-Si:H) solar cells with 1100 nm intrinsic μc-Si:H layer as well as amorphous/microcrystalline silicon (a-Si:H /μc-Si:H) tandem solar cells with 300 nm top intrinsic a-Si:H layer and 1100 nm intrinsic μc-Si:H layer, which were prepared by plasma enhanced chemical vapour deposition (PECVD) technique.

The thicknesses of ZnO:Al thin films are tested with surface profiler with the accuracy of 10 nm (Dektak 3030, Veeco Instruments Inc). The electrical properties of ZnO:Al thin films were characterized by Hall effect measurements. Diffuse and total transmissions (DT and TT) as well as total reflection (TR) and the absorption of ZnO:Al thin films were measured by a double-beam spectrophotometer with an integrating sphere (Perkin Elmer Lambda 19). In order to avoid the test error by the rough surface structures, the index matching liquid (CH_2I_2) was used during the TT and TR measurements [12]. The topographies of the samples were investigated by scanning electron microscopy (SEM, Supra 55VP SmartSEMTM, Carl Zeiss, Germany). The chemical compositions of sputtered ZnO:Al films were characterized by secondary ion mass spectroscopy (SIMS). The current-voltage (I-V) parameters of silicon thin films solar cells were measured with the sun simulator (WACOM-WXS-140S-Super) under the standard tested conditions (1000 W/m^2, AM1.5, 25°C).

2. Results and discussions

2.1 Influences of substrate temperature and discharge power on ZnO:Al films

Fig. 2 shows the dynamic deposition rates (DDRs) of ZnO:Al films deposited at different substrate temperatures and discharge powers as well as different working pressures (1.0 Pa and 1.5 Pa). ZnO:Al films deposited at a specific discharge power and different substrate temperatures show similar DDRs. It is also found that the DDR almost linearly increases from approximate 11 nm·m/min up to 90 nm·m/min with the enhanced discharge power from 2 kW to 14 kW. The thicknesses of all films are kept between 800 nm and 1000 nm. The normalized DDR is about 6 nm·m /(min·kW) here. Kim et al.[13] reported that the deposition rate decreased with the increasing substrate temperature due to thermal desorption of adatoms from substrate surface. However, such a kind of observation did not happen here, which could be due to the relatively higher working pressures (1.0 Pa and 1.5 Pa) compared to the working pressure of 2 mTorr (is approximately equal to 0.26 Pa) used in the reference [13]. Even though the substrate temperature seems not to strongly effect on the deposition rate, it leads to different electrical properties and grain structures as well as etching behaviors.

As shown in **Fig. 3**(a). the resistivity (ρ) drops from about $3.0\times10^{-3}\ \Omega\cdot$cm to about $5.0\times10^{-4}\ \Omega\cdot$cm with the increase of substrate temperatures from 225 °C to 350 °C for ZnO:Al films deposited at 4 kW and 14 kW as well as 1.5 Pa. Besides, the resistivity of the films deposited at 14 kW and a specific substrate temperature seems slightly lower than that of films deposited at 4 kW. Even though the ZnO:Al films deposited at 1.0 Pa as well as at 2 kW and 8 kW show the similar trend in resistivity, the high rate films (under 8 kW) at low substrate temperatures, for example at 250 °C, show a higher resistivity than that of low rate films (2 kW).

As can be seen in **Fig. 3**(b), the carrier concentration first increases and then decreases towards high substrate temperatures. The first increase in carrier concentration towards high substrate temperatures could be due to the excitation of aluminum dopant atoms. Differently, the decrease at very high substrate temperatures might be caused by desorption (or re-evaporation) of superfluous zinc atoms as well as aluminum impurity atoms, which will be discussed below. Similar dependence relationship can be found from ZnO:Al films reactively or non-reactively sputtered at

different substrate temperatures [8, 14]. Furthermore, the films deposited at high discharge powers like 8 kW and 14 kW show a lower carrier concentration compared to the films deposited at low discharge powers in this case. High discharge power may lead to the formation of alumina, which reduces the doping percent and results in a decrease in carrier concentration [15]. Moreover, the carrier concentration of ZnO:Al films prepared from the targets with the same doping level (0.5 wt%) is similar to the report by Berginski et al [8].

The dependence of carrier mobility (μ) of ZnO:Al films on substrate temperature is given in **Fig. 3**(c). The mobility increases with the enhanced substrate temperature. Highest mobility of up to 50 cm^2/Vs was achieved for low rate films deposited at 2 kW. Even for high rate films deposited at 14 kW, a high mobility of about 45 cm^2/Vs was obtained. It is a great advantage for such a kind of sputtering technique. The high substrate temperature leads to a high crystallizations of polycrystalline ZnO:Al films and then reduces the scattering of carrier (electron) at the grain boundaries [16-18]. Moreover, the hall mobility is expected to reduce when the substrate temperatures increases to an even higher temperature. Since high substrate temperatures could lead to the strong a re-evaporation of zinc atoms as well as the formation of alumina, which works as local defects and then results in the decrease of hall mobility [14, 15, 19-21]. In addition, the tensile stresses at high substrate temperatures, which are usually caused by grain boundary relaxation [22, 23], could be dominated compared to the compress stresses.

Fig. 4 shows the aluminum atom percent (Al/(Al+Zn)) i.e. C_{Al} measured with SIMS and carrier concentration measured with Hall effect measurement for ZnO:Al films deposited at 2 kW and different substrate temperatures. The Al to (Al+Zn) atom ratio in the ceramic targets is 0.792 at%. The ZnO:Al film deposited at 250 °C shows a high C_{Al} but a low carrier concentration. When substrate temperature reaches to 300 °C, the ZnO:Al film shows a low C_{Al} and a high carrier concentration as well. As the substrate temperature increases further, the carrier concentration decreases, which could be due to the decrease of C_{Al} in films as shown in **Fig. 4** . The observations above demonstrates that part of aluminum atoms at a low substrate temperature do not replaced the Zn atoms and thus have not contributed to doping as well as carrier concentration in ZnO film. High substrate temperature leads to a high doping [24] but in the mean while may results in a slight evaporation for aluminum atoms [14]. Compared to the doped level in the targets (0.792 at% C_{Al}), the C_{Al} values in films are much higher. It implies that much more

zinc atoms may be evaporated from film surface thanks to a high zinc evaporation pressure compared to aluminum atoms [14].

Fig. 5 shows that the etching rate of ZnO:Al film decreases with the increasing substrate temperatures. For the films deposited at 4 kW and 2 kW as well as different substrate temperatures in the range of 225-350 °C, the etching rate drops from ~11 nm/s to ~4 nm/s and from ~7 nm/s to ~2.5 nm/s, respectively. The films deposited at 8 kW and 14 kW present the high etching rates of up to 8 nm/s at the substrate temperatures of less than 300 °C. The etching rate dramatically drops to about 2 nm/s at high substrate temperatures. Additionally a higher working pressure leads to a higher etching rate as shown in **Fig. 5**. More details about the influence of working pressure on the etching behavior will be discussed in details in the following section.

By a chemical wet etching in HCl solution only films deposited at substrate temperatures of higher than 325 °C and 2 kW show crater-like surface structures as shown in **Fig. 6** (a), which are defined as Type B by Kluth et al. based on the modified Thornton model [7]. The high rate ZnO:Al films (HR-AZOs) deposited at 350 °C and 14 kW display the flat surfaces with a few craters on the surface as shown in **Fig. 6** (d) . Almost all films deposited substrate temperature of lower than 300 °C (except the film deposited at 2 kW and 300 °C), show Type A surface structures (hill-like structures with small feather sizes in diameter and depth) as shown in **Fig. 6** (c, e and f) . The film deposited at 2 kW and 300 °C, shows wide but shallow craters on the surface (see **Fig. 6** (b)), which would be generally regards as the Type C. However, such a kind of surface structure is different from the defined Type C. Since the etching rate of this type is much higher than that of the defined Type C and even higher than that of Type B as shown in **Fig. 5**. Thus we do think there exists a narrow transition zone between Type A region and Type B region, which was not observed and marked by Kluth et al [7].

The optical properties (TT and absorption as well as haze i.e. DT to TT ratio) of surface-textured low rate ZnO:Al films (LR-AZOs) deposited at 2 kW and HR-AZOs deposited at 14 kW are shown in **Fig. 7**. As can be seen in **Fig. 7** (a and b)**,** they show a high TT of more than 85% and a very low absorption close to zero in visible spectral region. Differently, the etched LR-AZOs (2 kW) prepared at 325 °C and 350 °C with large crater-like surface show high hazes of up to 70% at 700 nm. In addition, the LR-AZOs deposited at substrate temperatures of less than 300 °C display low hazes. Especially for the film deposited at 300 °C with large but shallow

craters, it shows a low haze. As to etched HR-AZOs they show high TT, low absorptions and very low hazes less than 30% at 700 nm irrespective of the surface textures.

2.2 Influences of working pressure and discharge power on ZnO:Al films

The DDRs of ZnO:Al films deposited at different working pressures and discharge powers are given in **Fig. 8**, where the lines are fits based on Keller-Simmons model [25-28]. Note that substrate temperature for all film depositions is 350°C. For LR-AZOs deposited at 2 kW, the highest DDR of 11 nm·m/min was obtained. The high DDR of up to 90 nm·m/min was achieved for high rate films deposited at 14 kW. For each series of samples in term of the specific discharges, the DDR tends to decrease with the increasing working pressures due to high particle collisions at high working pressures. As to the decrease of DDR at low working pressures, it is mainly caused by the re-sputtering of sputtered atoms from the film surface [25, 26]. Furthermore, the shift of DDR towards low values becomes profound at higher discharge powers. As shown in **Fig. 8**, the zero pressure-distance product $(pd)_0$ [27], which is the characteristic of the exponential decay of deposition rate with working pressure, increases from 55 Pa·cm to 165 Pa·cm with the enhanced discharge power from 2 kW to 14 kW. The high $(pd)_0$ value implies a high mean free path and therefore a slow decay of deposition rates. Similar relationship between $(pd)_0$ and deposition rate was observed by Drüsedau el al [27].

Fig. 9 shows the electrical properties of as-deposited ZnO:Al thin films as a function of working pressure. The resistivity initially decreases and then increases with the increase of the working pressure between 0.5-3 Pa for all series of ZnO:Al films. The minimal resistivity values of 3.4×10^{-4} Ω·cm and 3.6×10^{-4} Ω·cm for LR-AZOs deposited at 2 kW and 4 kW, respectively, are obtained at 1.5 Pa. For HR-AZOs deposited at high discharge powers like 14 kW, the minimum (3.8×10^{-4} Ω·cm) appears at a higher working pressure like at 2.0 Pa. Moreover, the HR-AZOs deposited at low working pressures display higher resistivity compared to L R-AZOs. However, the resistivity for all films here is in the range of 3.4×10^{-4} Ω·cm and 5.0×10^{-4} Ω·cm, which demonstrates a great advantage for such a sputtering technique.

The carrier concentration n is between 3.0×10^{20} cm^{-3} and 3.9×10^{20} cm^{-3} as shown in **Fig. 9**(b), which is in the range of carrier concentration reported by Berginski et al [8]. The very low

and high working pressure leads to slightly low carrier concentration and for these films. In the same way, the very low and high working pressure leads to slightly low mobility. Besides, the mobility at low working pressures for HR-AZOs is lower than that for LR-AZOs. A high mobility of up to 50 cm^2/Vs was achieved for LR-AZOs. Even for HR-AZOs, a high mobility of up to 46 cm^2/Vs was achieved. The low carrier concentration and low mobility may be related to the high energetic negative oxygen ion bombardment [20], which may lead to the formation of alumina and then results in a low doping level and a low carrier concentration [15, 29]. When the working pressure increases further, thermalization of sputtered particles through collision at high working pressures reduces diffusion energies of particles on film surface [13, 30]. As a result, grains of small size and more grain boundaries form in the ZnO:Al films, which results in a high scattering and then a decrease of carrier mobility.

As shown in **Fig. 10**, the etching rate of ZnO:Al films increases from 1.5 nm/s to about 9 nm/s with the increase of working pressures. For films deposited at low working pressures, they seem much more compact and etch-resistant. Moreover, the films deposited at high discharge powers display a relatively low etching rate at a specific working pressure.

By chemical wet etching, ZnO:Al films deposited at different discharge powers and working pressures show different surface structures as well. As an example, **Fig. 11** shows the surface structure of etched films deposited at different working pressures as well as 2 kW (LR-AZO: a, b, c and d) and 14 kW (HR-AZO: e, f, g and h). The LR-AZO films deposited at 0.5 Pa and 1.0 Pa display regular surface structure Type B, with the feather sizes of 1-2 μm in diameter and about 450 nm in depth (see **Fig. 11**(a)). The film prepared at 1.5 Pa shows a relatively flat surface with only a few large but shallow craters on the surface as shown in **Fig. 11**(b), which is similar to Type C (low etching rate, only a few large and shallow craters distributing on the surface) [7]. Based above result s, such a structure exists in the transition zone between Type A and Type B as mentioned above. With the increase of working pressure, the corresponding ZnO:Al films turn into hill-like surface textures as shown in **Fig. 11**(c and d). For the HR-AZOs, they all show flat surfaces and no Type B textured surface appear, which could be due to the influence of high discharge power. We can conclude that there is only a narrow deposition condition window for formation of Type B ZnO:Al films. As a matter of fact, the textured surface of ZnO:Al films after etching depends on not only substrate temperature and working pressure but also discharge power as well as other

conditions like oxygen partial pressure [10].

As pointed out above, the etching behaviors are strongly related with the grain structures. However, it is not clear about the exact relationship between them so far. Maki et al. [31] studied the chemical wet behaviors on single crystal ZnO (001) polar surfaces i.e. Zn-terminal surface and O-terminal surface. After etching in HCl solution, the hexagonal pit shape formed. In fact, Hüpkes et al. also reported different surface structures by etching single crystal ZnO from Zn-terminal surface and O-terminal surface [32, 33]. However, for polycrystalline ZnO:Al the etching behavior is much more complex. Different deposition conditions lead to the formation of different surface textures after the chemical wet etching treatment.

Similar to the temperature series of thin films mentioned above, LR-AZOs and HR-AZOs deposited at different working pressures show high TT and low absorptions as shown in **Fig. 12** (a and b). As shown in **Fig. 12** (c) etched LR-AZOs deposited at 0.5 Pa and 1.0 Pa show high hazes of up to 70% at 700 nm, whose surface textures belong to Type B. But the LR-AZOs deposited at pressures of more than 1.5 Pa show low haze. For etched HR-AZOs, they present low hazes of less than 30% at 700 nm. Thus it is a challenge for us to improve the surface structure of HR-AZOs.

2.3 Solar cells

Surface-textured LR-AZO (2 kW, 350°C) and HR-AZO (14 kW, 350°C) films were applied in μc-Si:H solar cells as front contact electrodes and the corresponding I-V results of solar cells are listed in **Table I**. For the cells A1-A5 with LR-AZO as front contacts, the highest conversion efficiency η of 8.5 % were achieved for solar cell A2 on crater-shape ZnO:Al film deposited at 1 Pa due to and a relatively high short current density (J_{sc}) of 22.9 mA/cm^2 and a relatively high fill factor (FF) 71.4%. For cell A4 and A5 with the LR-AZO front contacts of hill-like surface structure, low FF values of 64-65 % and low V_{oc} of 0.49-0.50 V were obtained. However, the relatively high J_{sc} of higher than 21 mA/cm^2 were still achieved. The cell A3 with relatively flat LR-AZO front contact shows a high FF but a low J_{sc} due to a low light scattering or light trapping effect, which are similar to the cells B1-B4 with HD-AZO front contact as shown in the **Table I**. Differently, the cell A1 with largest crater LR-AZO front contact (SEM image is not shown here)

shows a highest J_{sc} of 23.3 mA/cm^2 but a relatively lower FF compared to the cells A2 and A3. The low FF could be due to the formation of micro-voids in the μc-Si:H solar cells grown on deep valley ZnO front contact [34-36] even though good light trapping effect (or high haze) and high J_{sc} are obtained. By dry plasma treatment or coating with a nano-scalar on the textured ZnO front contact, FF could be effectively improved [34, 37]. Moreover, reducing the feature sizes of craters of textured ZnO front contact, for example by decreasing chemical wet etching time, is also expected to improve the FF.

Furthermore, the crater-shape LR-AZO film (2 kW, 350°C, 1.0 Pa) was used for preparation of a-Si:H /μc-Si:H tandem solar cell and higher efficiency of 11.3% had been achieved. However, it seems that the FF is still low [38], which could be also due to the defects i.e. micro-voids in the bottom μc-Si:H materials [34-36]. Thus more works should be carried out to improve the FF of tandem solar cells in the near future.

As to the solar cells with ZnO:Al substrates of low temperatures, they show low FF, high J_{sc} and resulting low efficiencies (not shown here), which are similar to the solar cells with ZnO:Al substrates deposited at high substrate temperatures and high working pressures (Cells A4, A5 and A6) because of the similar surface structures as compared in **Fig. 6** and **Fig. 11**.

As seen from cells A3 and B1-B4, ZnO:Al front contacts with flat surface structure result in a high FF but a low J_{sc} for the corresponding μc-Si:H solar cells. However, a novel two-step etching method combining the HF etching and HCl etching for these flat ZnO:Al films could effectively improve the surface structures as well as light scattering properties and corresponding high efficiency solar cells (11%) have been achieved in our group [39, 40].

3. Conclusions

In this study, ZnO:Al films deposited from dual rotatable ceramic targets are systematically investigated. The influences of substrate temperature and working pressure as well as discharge power on ZnO:Al films were studied. In addition to the substrate temperature and working pressure, the discharge power plays an important role in different properties of magnetron sputtered ZnO:Al films here including optical and electrical properties, deposition rate, surface structure and etching behavior. A high carrier mobility of about 45 Vs/cm^2 for HR-AZO films of

up to 90 nm·m/min are obtained, which is close to the highest carrier mobility (50 Vs/cm^2) of LR-AZO films. The sputtered ZnO:Al films show different surface structures after a chemical wet etching process, which strongly rely on different deposition conditions such as substrate temperature, working pressure and discharge power here. However, there is only a narrow parameters window i.e. low discharge power, high substrate temperature and low working pressure for sputtered ZnO:Al films to achieve a good surface structure (Type B) after a chemical wet etching process based on the observations in this study. However, for the etched ZnO:Al film with relatively flat surface structure, they can be improved through a novel two-step etching method of HF etching plus HCl etching. The surface-textured ZnO:Al films were applied in silicon thin film solar cells and higher efficiencies of 8.5% and 11.3% are achieved for single junction μc-Si:H solar cells and a-Si:H /μc-Si:H tandem solar cell, respectively.

Acknowledgements

The authors would like to thank H. Siekmann, J. Worbs for extensive technical support. We also would like to thank H. B. Bochen for SEM measurement and U. Zastrow for his great efforts in SIMS measurement.

References

[1] B. Rech, H. Wagner, Applied Physics a-Materials Science & Processing 69/2 (1999) 155.

[2] H. Keppner, J. Meier, P. Torres, D. Fischer, A. Shah, Applied Physics a-Materials Science & Processing 69/2 (1999) 169.

[3] J. Müller, O. Kluth, S. Wieder, H. Siekmann, G. Schope, W. Reetz, O. Vetterl, D. Lundszien, A. Lambertz, F. Finger, B. Rech, H. Wagner, Solar Energy Materials and Solar Cells 66/1-4 (2001) 275.

[4] J. Müller, G. Schope, O. Kluth, B. Rech, M. Ruske, J. Trube, B. Szyszka, X. Jiang, G. Brauer, Thin Solid Films 392/2 (2001) 327.

[5] O. Kluth, B. Rech, L. Houben, S. Wieder, G. Schope, C. Beneking, H. Wagner, A. Loffl, H.W. Schock, Thin Solid Films 351/1-2 (1999) 247.

[6] J.I. Owen, Photovoltaics (IEK-5), Institute of Energy and Climate Research (IEK), Forschungszentrum Jülich GmbH, RWTH Aachen University, Aachen, 2011.

[7] O. Kluth, G. Schöpe, J. Hüpkes, C. Agashe, J. Müller, B. Rech, Thin Solid Films 442/1-2 (2003) 80.

[8] M. Berginski, J. Hüpkes, M. Schulte, G. Schöpe, H. Stiebig, B. Rech, M. Wuttig, Journal of Applied Physics 101/7 (2007) 074903_1.

[9] M. Berginski, B. Rech, J. Hüpkes, H. Stiebig, M. Wuttig, SPIE Photonics, Strasbourg, France, 2006.

[10] H. Zhu, J. Hüpkes, E. Bunte, S.M. Huang, Applied Surface Science 256 (2010) 4601.

[11] H. Zhu, J. Hüpkes, E. Bunte, S.M. Huang, Surface & Coatings Technology 205 (2010) 773.

[12] M. Mizuhashi, Y. Gotoh, K. Adachi, Japanese Journal of Applied Physics Part 1-Regular Papers Short Notes & Review Papers 27/11 (1988) 2053.

[13] K.H. Kim, K.C. Park, D.Y. Ma, Journal of Applied Physics 81/12 (1997) 7764.

[14] B. Szyszka, Thin Solid Films 351/1-2 (1999) 164.

[15] T. Minami, H. Nanto, S. Takata, Japanese Journal of Applied Physics Part 2-Letters 23/5 (1984) L280.

[16] R.L. Petritz, Physical Review 104/6 (1956) 1508.

[17] K.L. Chopra, S. Major, D.K. Pandya, Thin Solid Films 102/1 (1983) 1.

[18] J.W. Orton, M.J. Powell, Reports on Progress in Physics 43/11 (1980) 1263.

[19] T. Minami, H. Sato, H. Nanto, S. Takata, Japanese Journal of Applied Physics Part 2-Letters 24/10 (1985) L781.

[20] K. Tominaga, K. Kuroda, O. Tada, Japanese Journal of Applied Physics Part 1-Regular Papers Short Notes & Review Papers 27/7 (1988) 1176.

[21] T. Minami, H. Sato, T. Sonoda, H. Nanto, S. Takata, Thin Solid Films 171/2 (1989) 307.

[22] C. David, T. Girardeau, F. Paumier, D. Eyidi, B. Lacroix, N. Papathanasiou, B.P. Tinkham, P. Guerin, M. Marteau, J. Phys.: Condens. Matter 23 (2011) 3343209.

[23] H.W. Lee, S.P. Lau, Y.G. Wang, B.K. Tay, H.H. Hng, Thin Solid Films 458/1-2 (2004) 15.

[24] B. Szyszka, V. Sittinger, X. Jiang, R.J. Hong, W. Werner, A. Pflug, M. Ruske, A. Lopp, Thin Solid Films 442/1-2 (2003) 179.

[25] O. Kappertz, R. Drese, J.M. Ngaruiya, M. Wuttig, Thin Solid Films 484/1-2 (2005) 64.

[26] J.M. Ngaruiya, O. Kappertz, S.H. Mohamed, M. Wuttig, Applied Physics Letters 85/5 (2004) 748.

[27] T.P. Drüsedau, M. Löhmann, B. Garke, Journal of Vacuum Science & Technology a-Vacuum Surfaces and Films 16/4 (1998) 2728.

[28] O. Kappertz, R. Drese, M. Wuttig, Journal of Vacuum Science & Technology a-Vacuum Surfaces and Films 20/6 (2002) 2084.
[29] I. Petrov, V. Orlinov, A. Misiuk, Thin Solid Films 120/1 (1984) 55.
[30] J.A. Thornton, Journal of Vacuum Science & Technology a-Vacuum Surfaces and Films 4/6 (1986) 3059.
[31] H. Maki, T. Ikoma, I. Sakaguchi, N. Ohashi, H. Haneda, J. Tanaka, N. Ichinose, Thin Solid Films 411/1 (2002) 91.
[32] K. Ellmer, A. Klein, B. Rech, Transparent Conductive Zinc Oxide ‐ Basics and Applications in Thin Film Solar Cells, Springer, Berlin, 2008.
[33] J. Hüpkes, J.I. Owen, S.E. Pust, E. Bunte, ChemPhysChem 13 (2012) 66.
[34] J. Bailat, D. Domine, R. Schluchter, J. Steinhauser, S. Fay, F. Freitas, C. Bucher, L. Feitknecht, X. Niquille, T. Tscharner, A. Shah, C. Ballif, Ieee, High-efficiency p-i-n microcrystalline and micromorph thin film silicon solar cells deposited on LPCVD ZnO coated glass substrates, Ieee, New York, 2006.
[35] M. Python, O. Madani, D. Domine, F. Meillaud, E. Vallat-Sauvain, C. Ballif, Solar Energy Materials and Solar Cells 93/10 (2009) 1714.
[36] F. Meillaud, A. Feltrin, D. Domine, P. Buehlmann, M. Python, G. Bugnon, A. Billet, G. Parascandolo, J. Bailat, S. Fay, N. Wyrsch, C. Ballif, A. Shah, Philosophical Magazine 89/28-30 (2009) 2599.
[37] O. Kluth, J. Kalas, M. Fecioru-Morariu, P.A. Losio, J. Hoetzel, The 26th European Photovoltaic Solar Energy Conference and Exhibition, Hamburg, Germany, 2011, p. 2354.
[38] B. Rech, T. Roschek, T. Repmann, J. Muller, R. Schmitz, W. Appenzeller, Thin Solid Films 427/1-2 (2003) 157.
[39] E. Bunte, H. Zhu, J. Hüpkes, J. Owen, EPJ Photovoltaics 2 (2011) 20602.
[40] H. Zhu, J. Hüpkes, E. Bunte, J. Owen, S.M. Huang, Sol. Energy. Mater.Sol.Cells 95 (2011) 964.

Captions

Fig. 1 Schematic of rotatable dual magnetron sputtering system**.**

Fig. 2 Dependence of dynamic deposition rate (DDR) of ZnO:Al films on substrate temperature and discharge power.

Fig. 3 Resistivity (a), carrier concentration (b) and mobility (c) of ZnO:Al films as a function of substrate temperature. The lines are guides for the eyes.

Fig. 4 Aluminum atom concentration (Al/(Al+Zn)) measured with SIMS and carrier concentration measured with Hall effect measurement for films deposited at 2 kW and different substrate temperatures from ceramic targets with an atom ratio of Al to (Al+Zn) of 0.792 at% or an aluminum oxide weight percent of 0.5 wt%.

Fig. 5 Etching rate of ZnO:Al films as a function of substrate temperature.

Fig. 6 Surface structures of after-etched ZnO:Al films deposited at 2 kW (left) and 14 kW (right) as well as different substrate temperatures: (a) 2 kW, 350°C, (b) 2 kW, 300°C, (c) 2 kW, 250°C, (d) 14 kW, 350°C, (e) 14 kW, 300°C, (f) 14 kW, 250°C,,

Fig. 7 Transmission and absorption as well as haze of textured ZnO:Al films deposited at 2 kW (a and b), 14 kW (c and d), respectively, and different substrate temperatures as well as other corresponding deposition conditions.

Fig. 8 Dependence of deposition rate of ZnO:Al films on working pressure and discharge power. The lines are fits based on Keller-Simmons model [25-28].

Fig. 9 Resistivity (a), carrier concentration (b) and mobility (c) of ZnO:Al films as a function of working pressure. The lines are the guides for the eyes.

Fig. 10 Etching rate of ZnO:Al films as a function of working pressure.

Fig. 11 Surface structures of etched ZnO:Al films deposited at different working pressures of 0.5-3 Pa as well as different discharge powers by a chemical wet etching step in diluted HCl solution (0.5%).

Fig. 12 Transmission and absorption of textured ZnO:Al films deposited at 2 kW (a) and 14 kW (b), as well as haze respectively, and different working pressure as well as other corresponding deposition conditions.

Table I The I-V results of silicon thin film solar cells with the LR-AZO (2 kW) and HR-AZO (14 kW) films as front contact electrodes. The types of silicon thin film solar cells as well as the deposition conditions of ZnO:Al films are described as well.

Figure 1

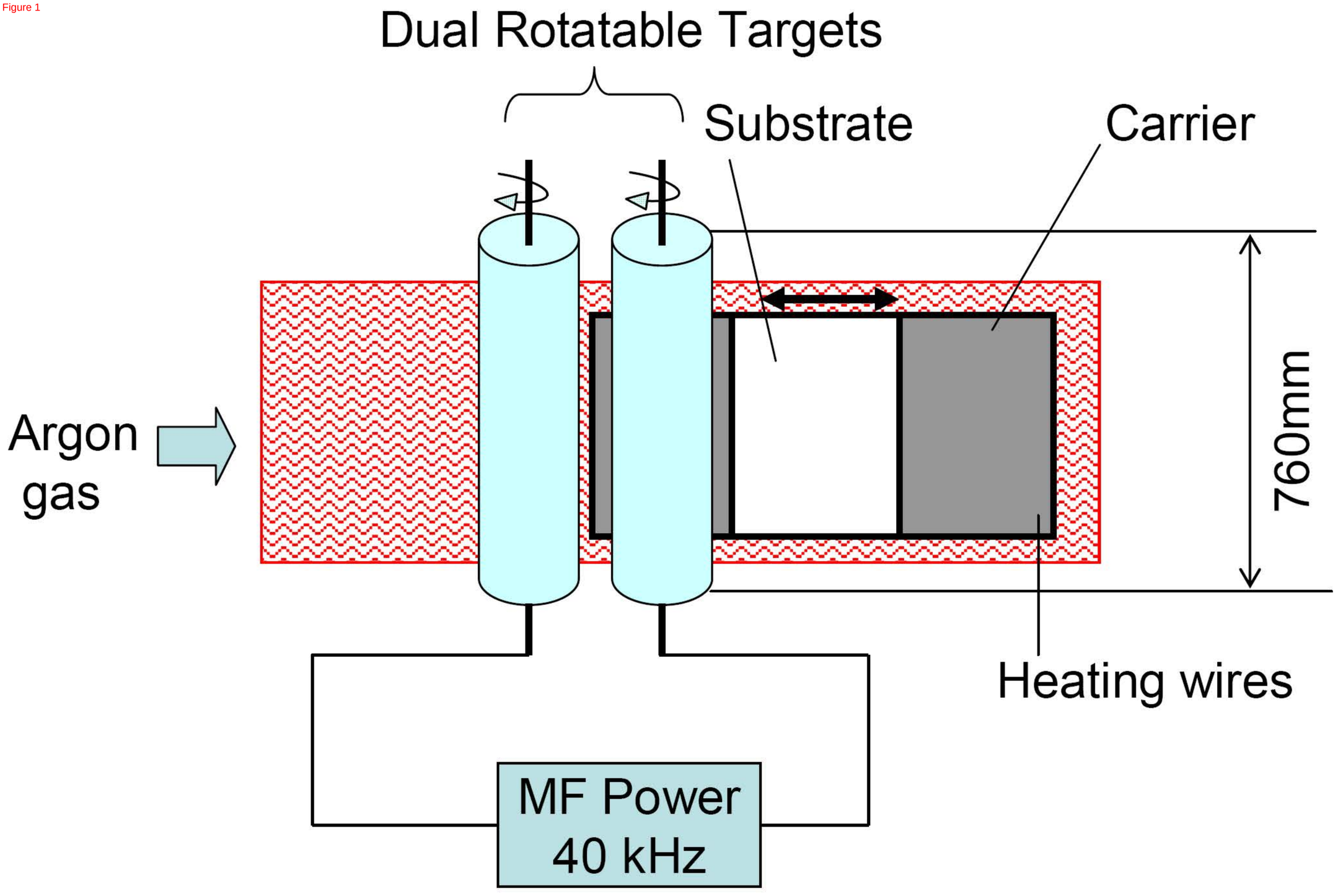
Dual Rotatable Targets
Substrate
Carrier
Argon gas
760mm
Heating wires
MF Power
40 kHz

Figure 2

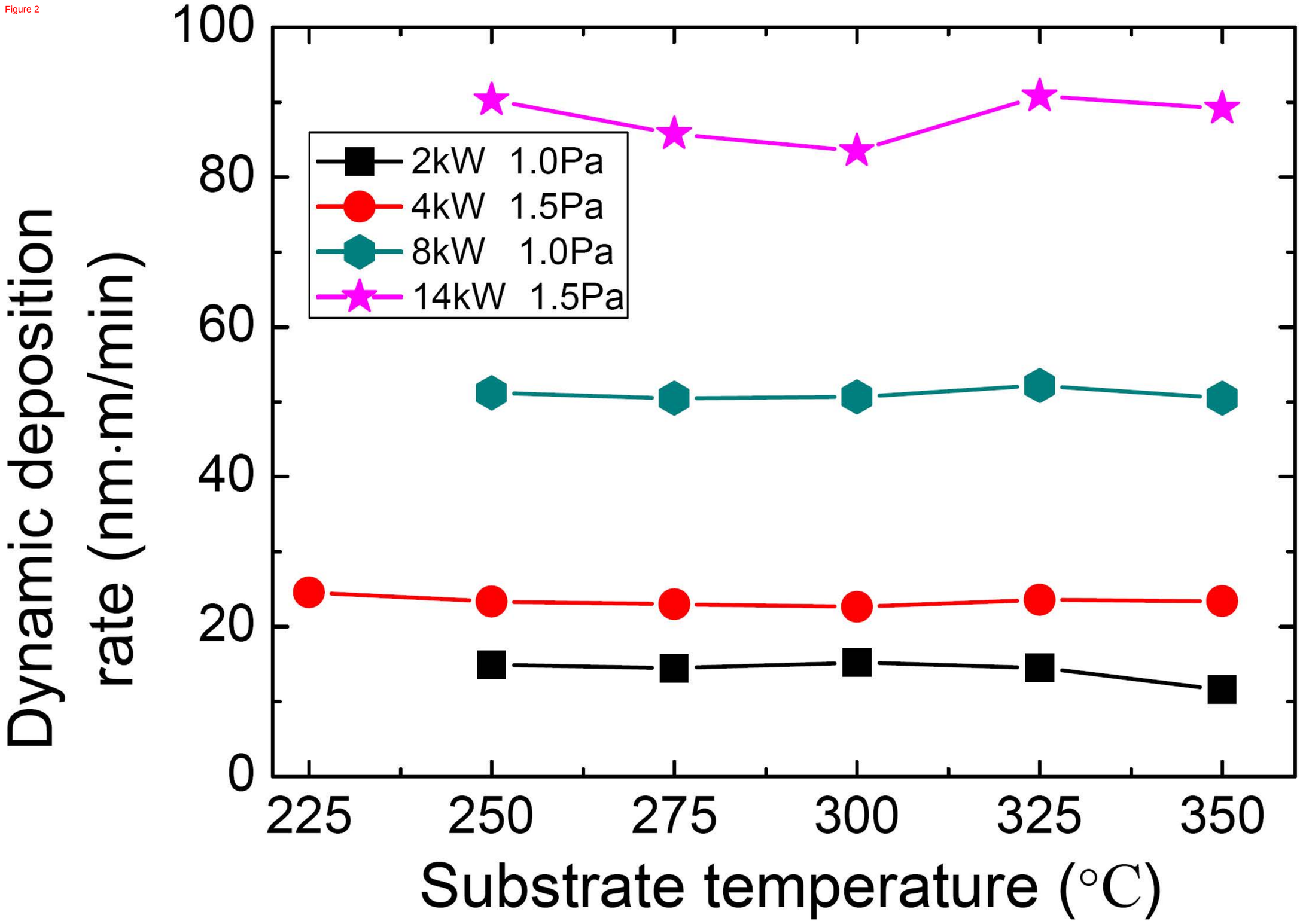
100
80
60
40
20
0
225
250
275
300
325
350
2kW 1.0Pa
4kW 1.5Pa
8kW 1.0Pa
14kW 1.5Pa
Dynamic deposition rate (nm·m/min)
Substrate temperature (°C)

Figure 3

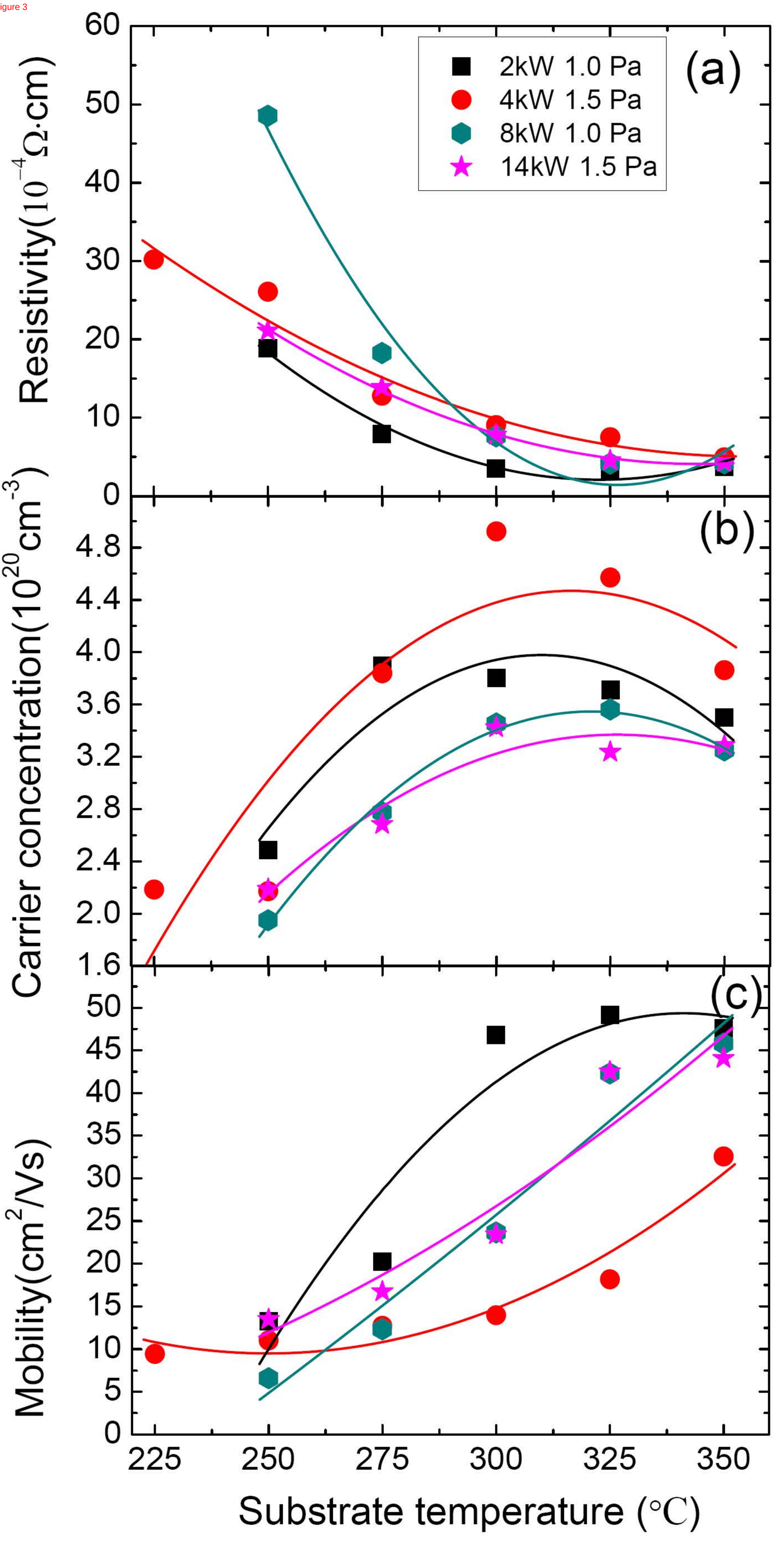
2kW 1.0 Pa
4kW 1.5 Pa
8kW 1.0 Pa
14kW 1.5 Pa
(a)
(b)
(c)
Resistivity($10^{-4}\Omega$·cm)
Carrier concentration(10^{20}cm^{-3})
Mobility(cm^2/Vs)
Substrate temperature (℃)
0
10
20
30
40
50
60
1.6
2.0
2.4
2.8
3.2
3.6
4.0
4.4
4.8
0
5
10
15
20
25
30
35
40
45
50
225
250
275
300
325
350

Figure 4

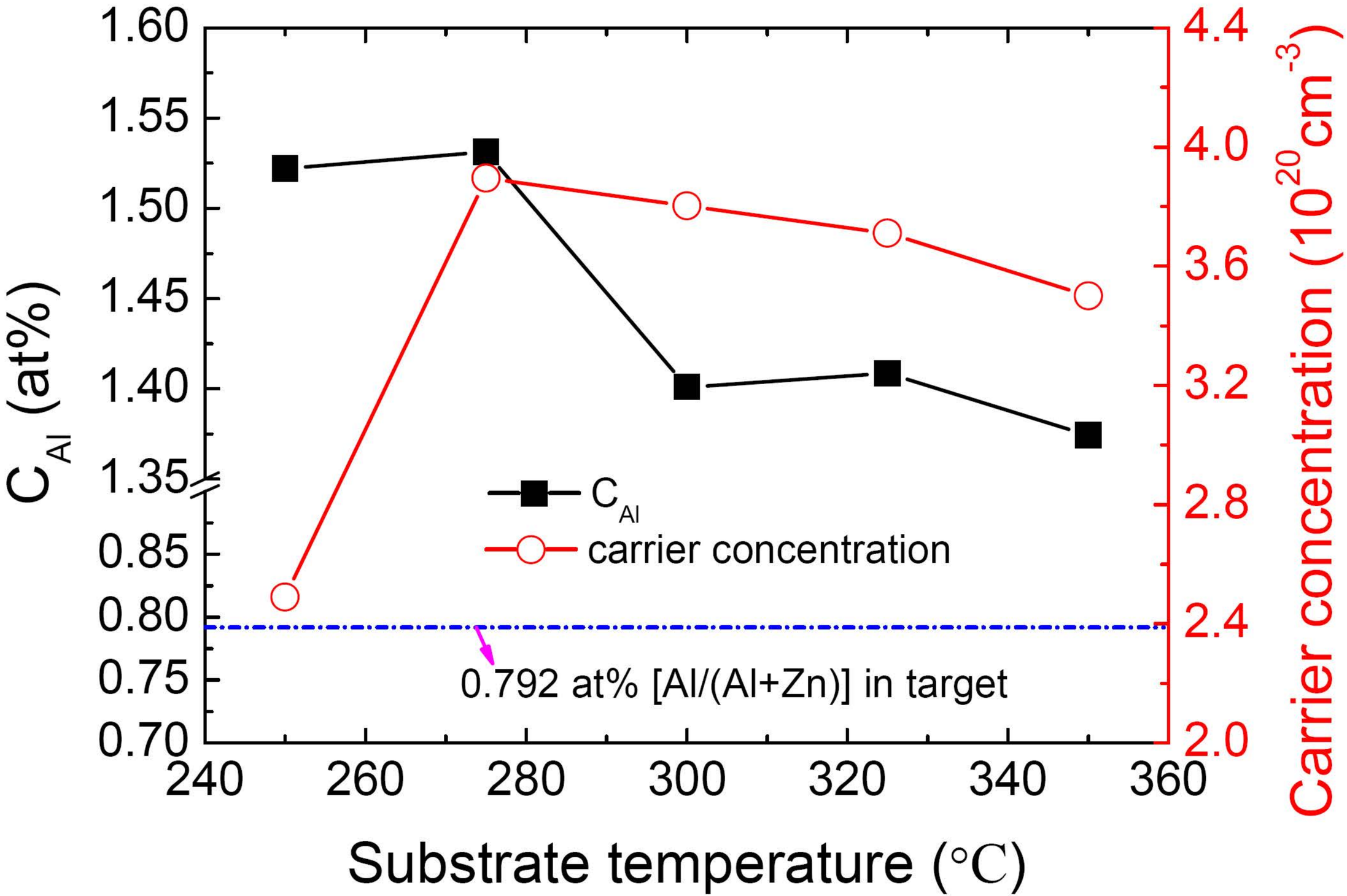
1.60
1.55
1.50
1.45
1.40
1.35
0.85
0.80
0.75
0.70
C_{Al} (at%)
4.4
4.0
3.6
3.2
2.8
2.4
2.0
Carrier concentration ($10^{20}cm^{-3}$)
C_{Al}
carrier concentration
0.792 at% [Al/(Al+Zn)] in target
240
260
280
300
320
340
360
Substrate temperature (°C)

Figure 5

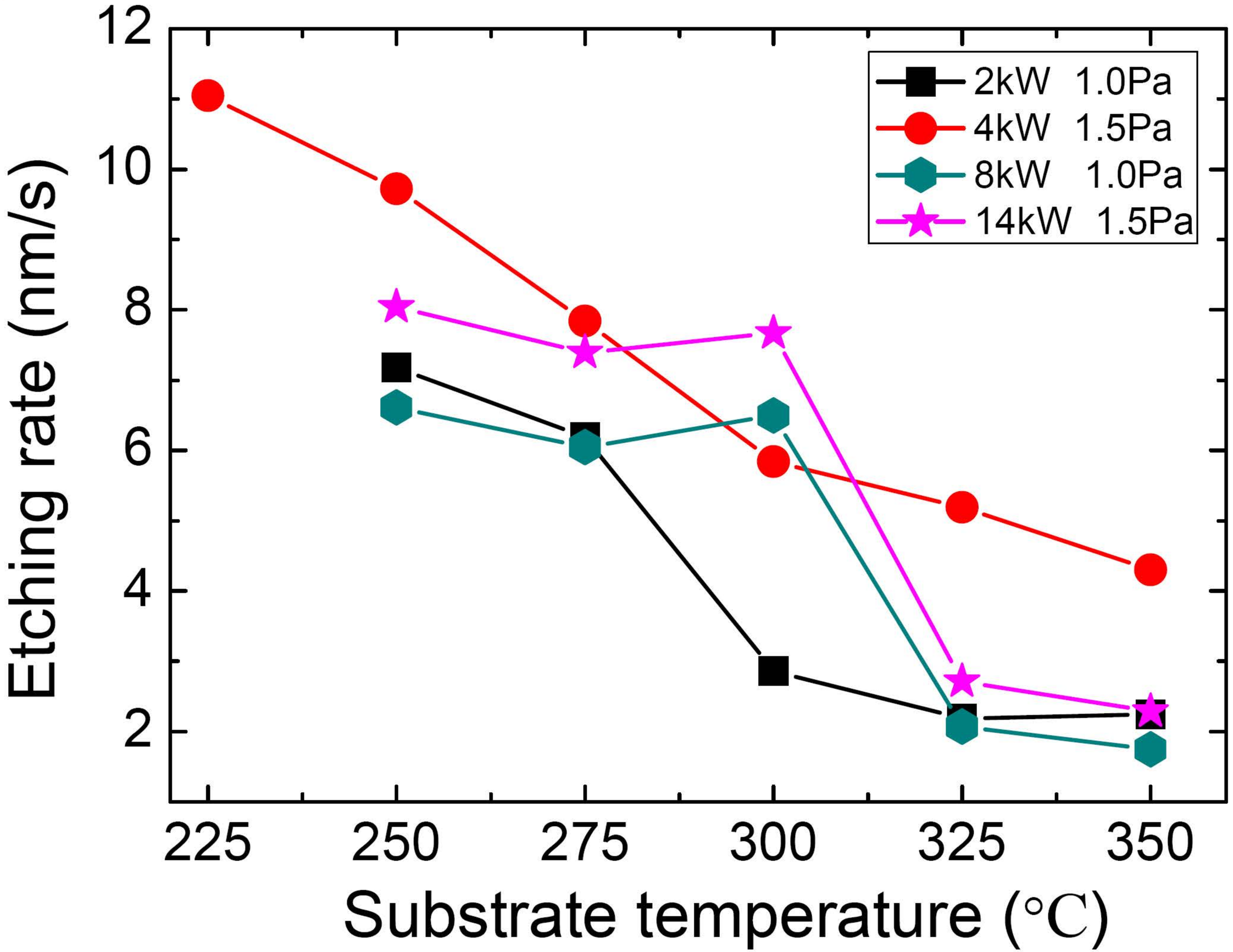
12
10
8
6
4
2
Etching rate (nm/s)
2kW 1.0Pa
4kW 1.5Pa
8kW 1.0Pa
14kW 1.5Pa
225
250
275
300
325
350
Substrate temperature (°C)

Figure 6

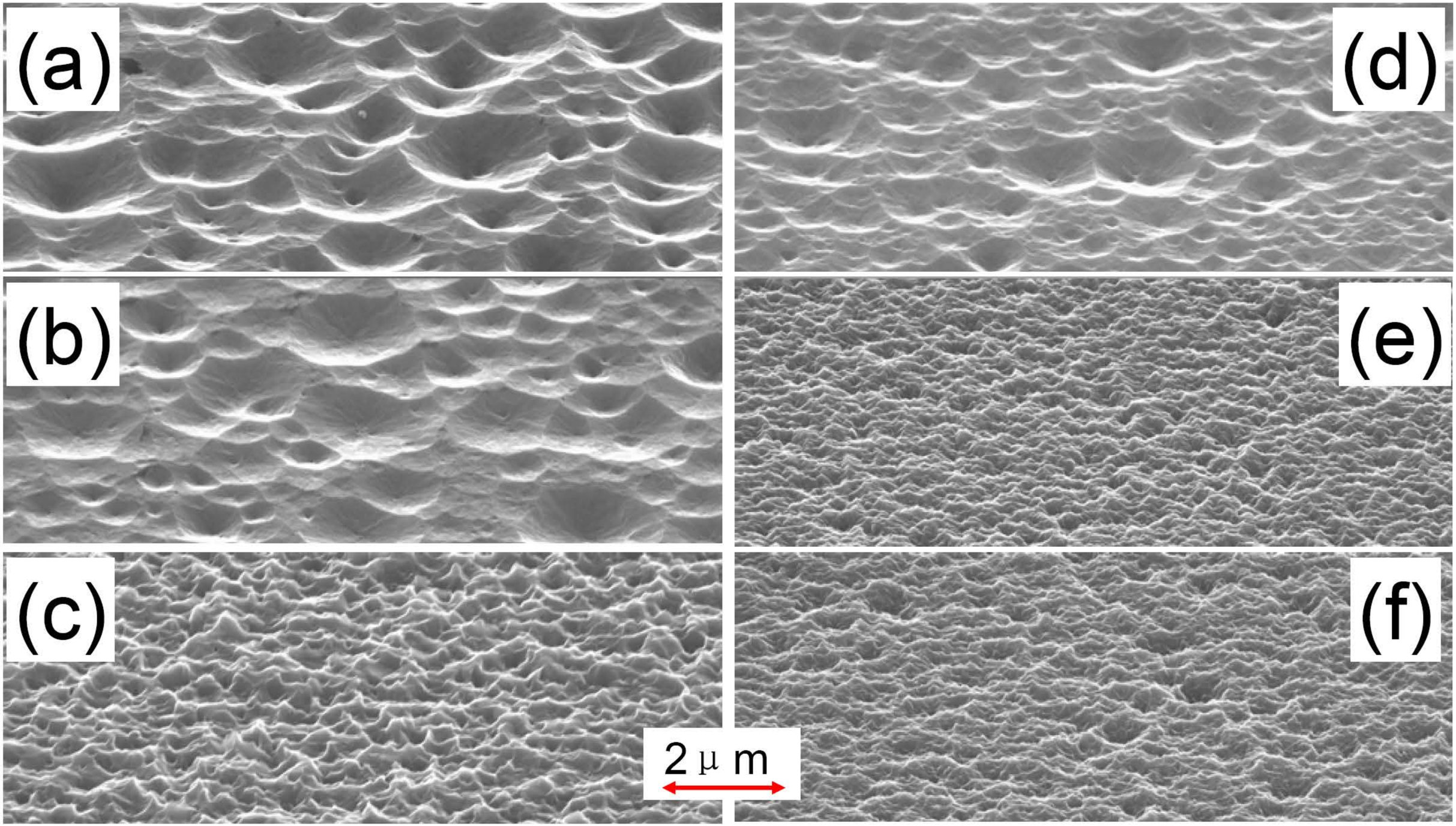

Figure 7

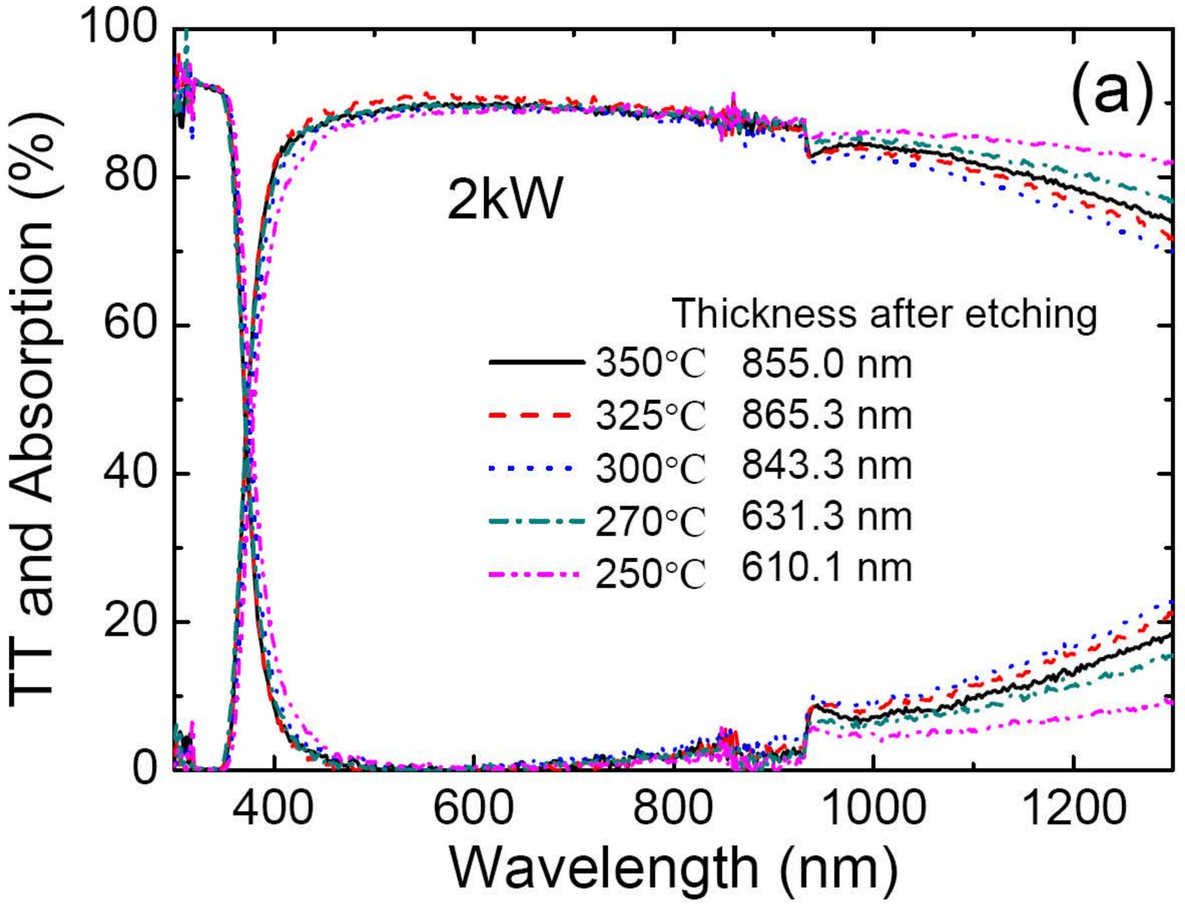
(a)
2kW
Thickness after etching
350℃ 855.0 nm
325℃ 865.3 nm
300℃ 843.3 nm
270℃ 631.3 nm
250℃ 610.1 nm
TT and Absorption (%)
Wavelength (nm)

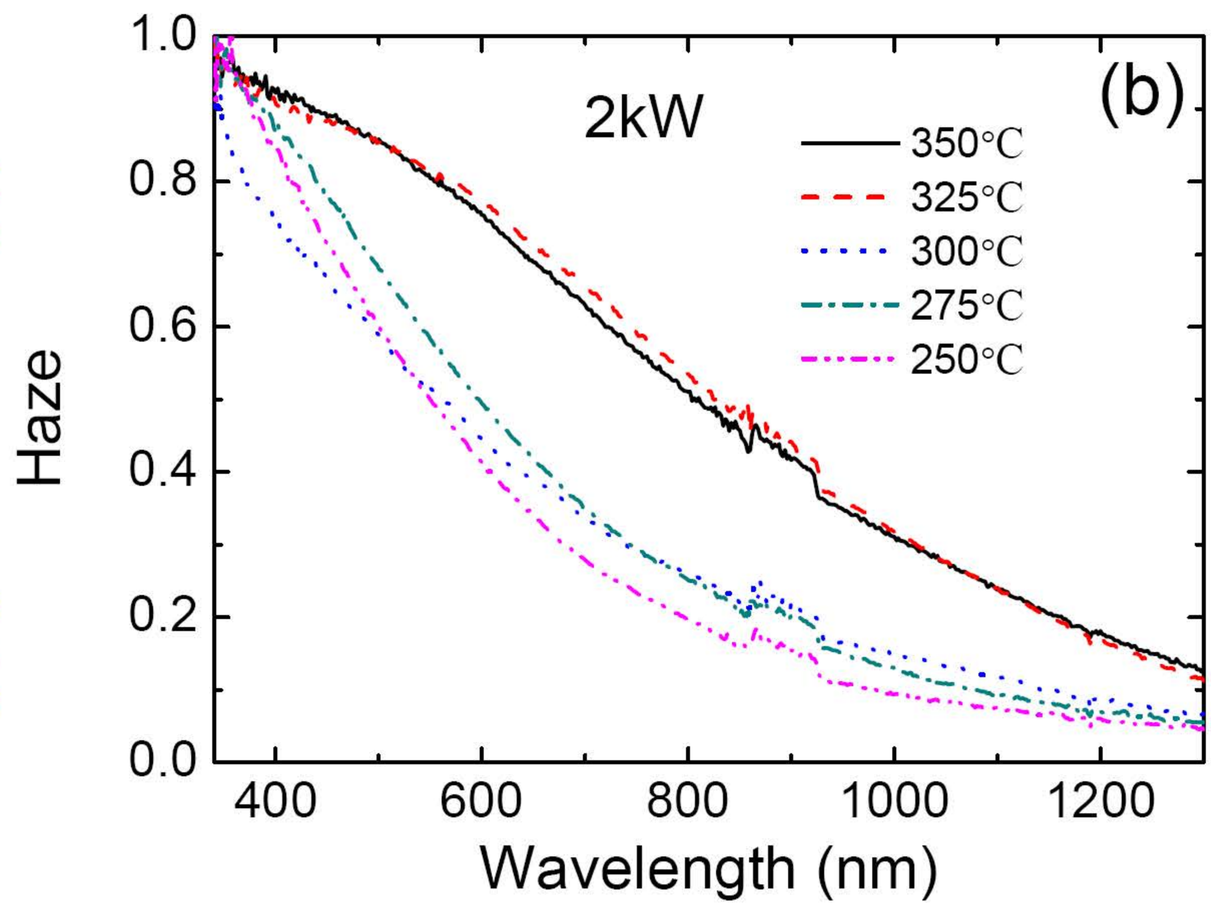
(b)
2kW
350℃
325℃
300℃
275℃
250℃
Haze
Wavelength (nm)

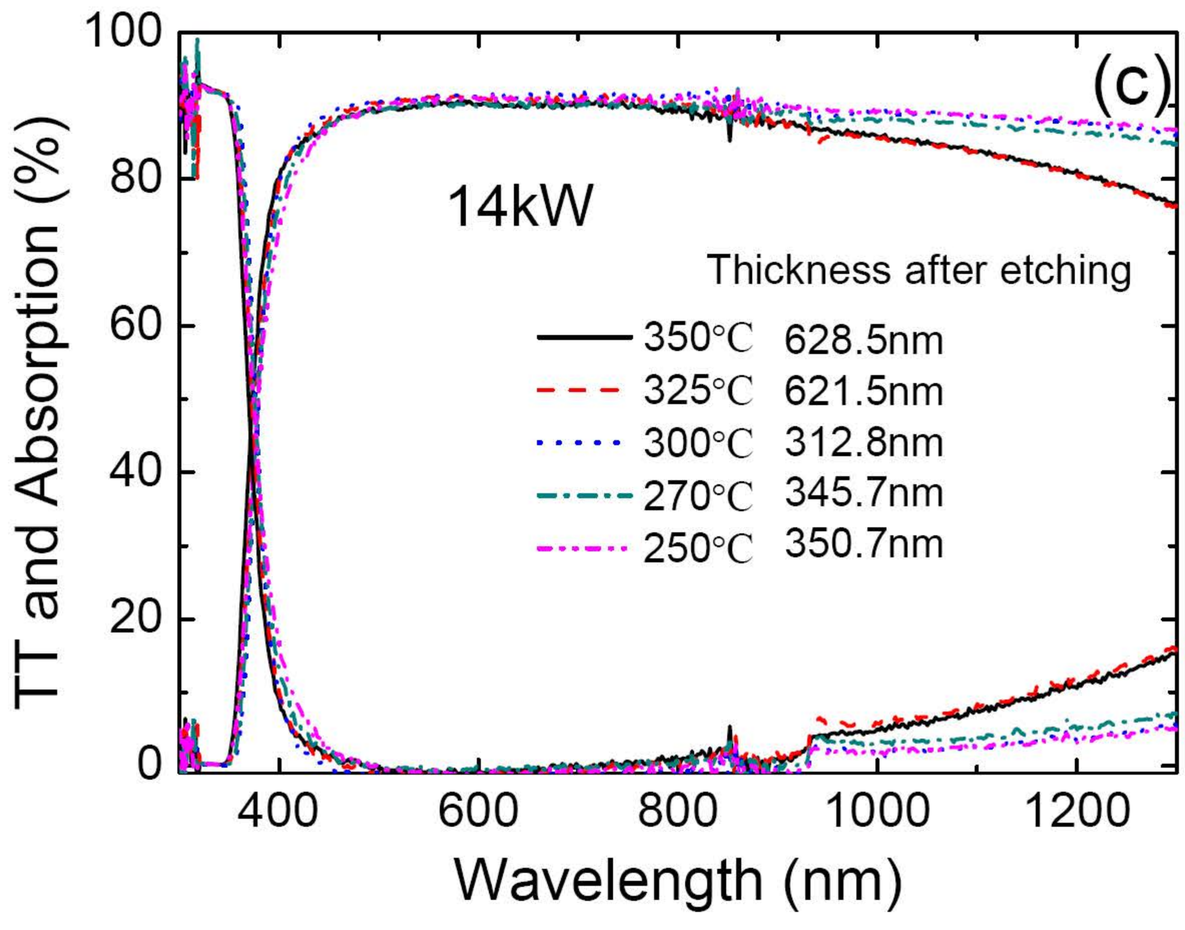
(c)
14kW
Thickness after etching
350℃ 628.5nm
325℃ 621.5nm
300℃ 312.8nm
270℃ 345.7nm
250℃ 350.7nm
TT and Absorption (%)
Wavelength (nm)

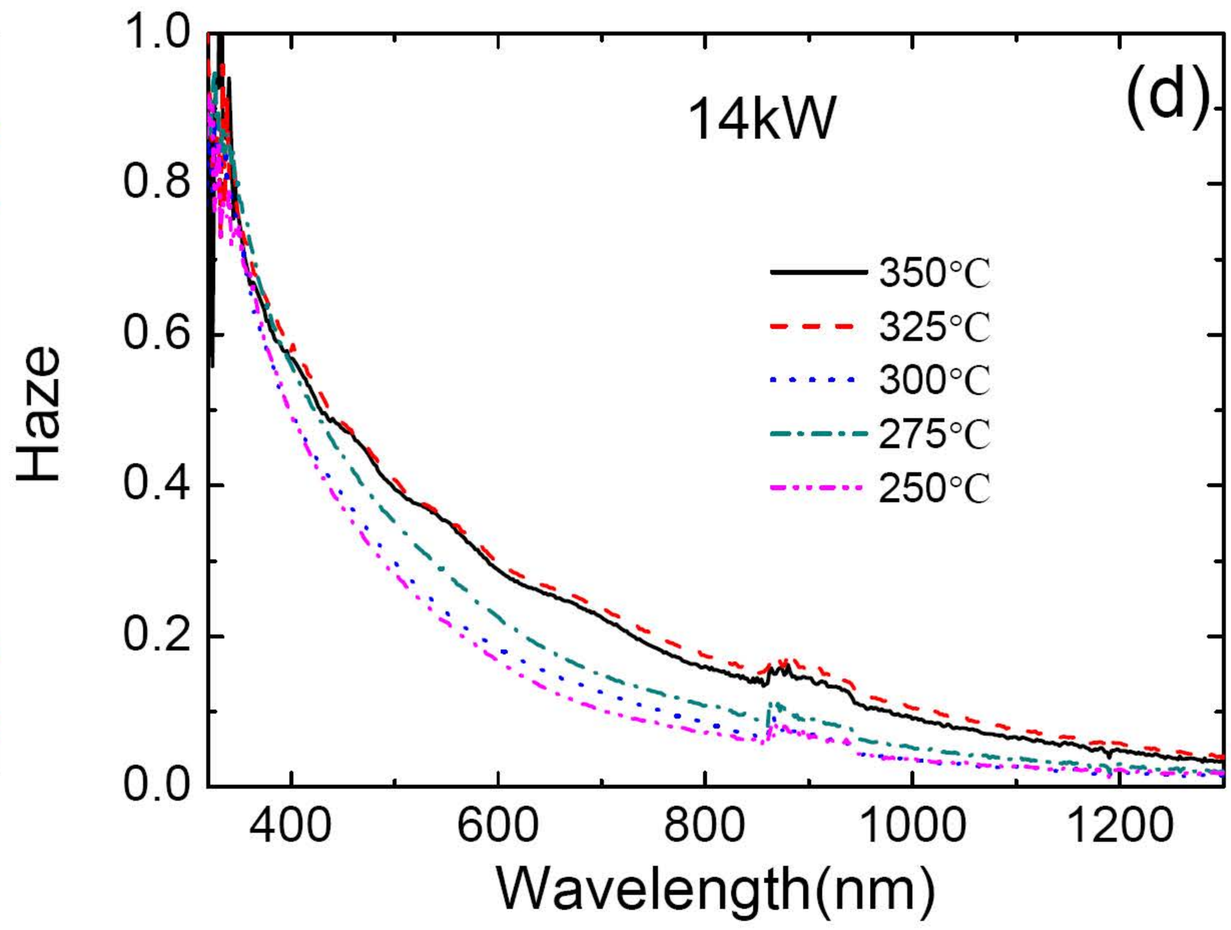
(d)
14kW
350℃
325℃
300℃
275℃
250℃
Haze
Wavelength(nm)

Figure 8

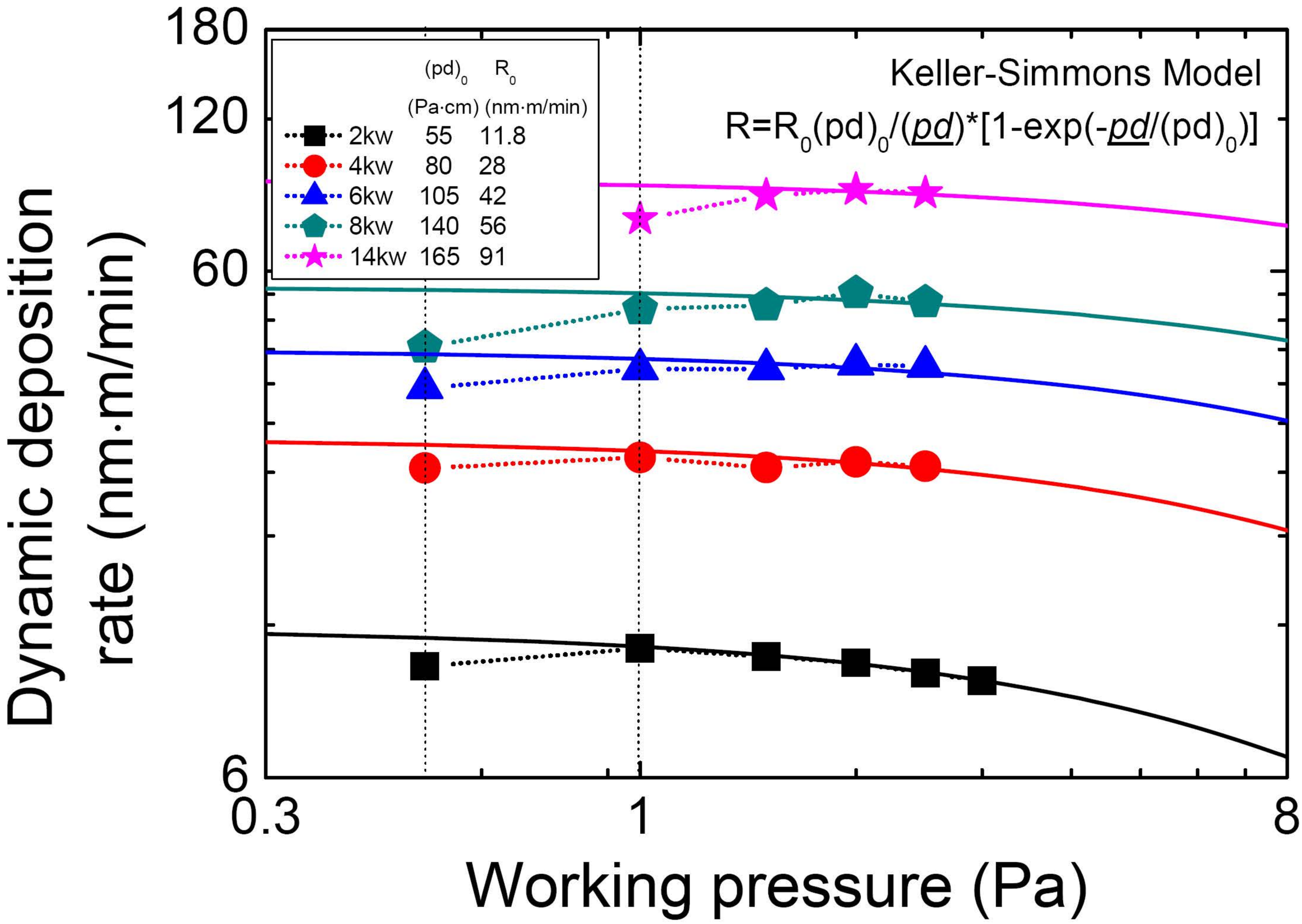
Keller-Simmons Model
R=R0(pd)0/(pd)*[1-exp(-pd/(pd)0)]
(pd)0 R0
(Pa·cm) (nm·m/min)
2kw 55 11.8
4kw 80 28
6kw 105 42
8kw 140 56
14kw 165 91
Dynamic deposition rate (nm·m/min)
180
120
60
6
0.3
1
8
Working pressure (Pa)

Figure 9

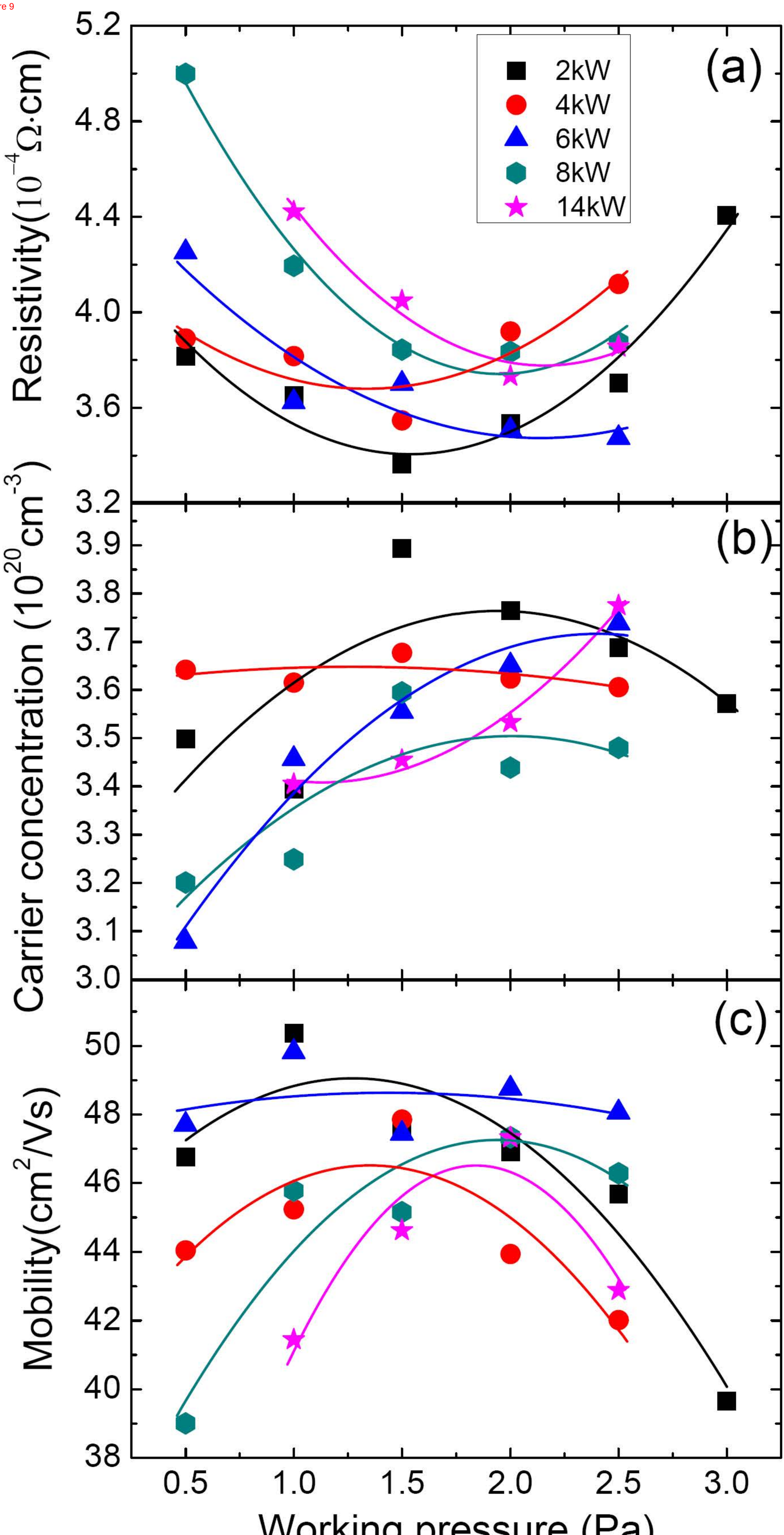
(a)
2kW
4kW
6kW
8kW
14kW
Resistivity($10^{-4}\Omega$·cm)
5.2
4.8
4.4
4.0
3.6
3.2
(b)
Carrier concentration (10^{20}cm^{-3})
3.9
3.8
3.7
3.6
3.5
3.4
3.3
3.2
3.1
3.0
(c)
Mobility(cm^2/Vs)
50
48
46
44
42
40
38
0.5
1.0
1.5
2.0
2.5
3.0
Working pressure (Pa)

Figure 10

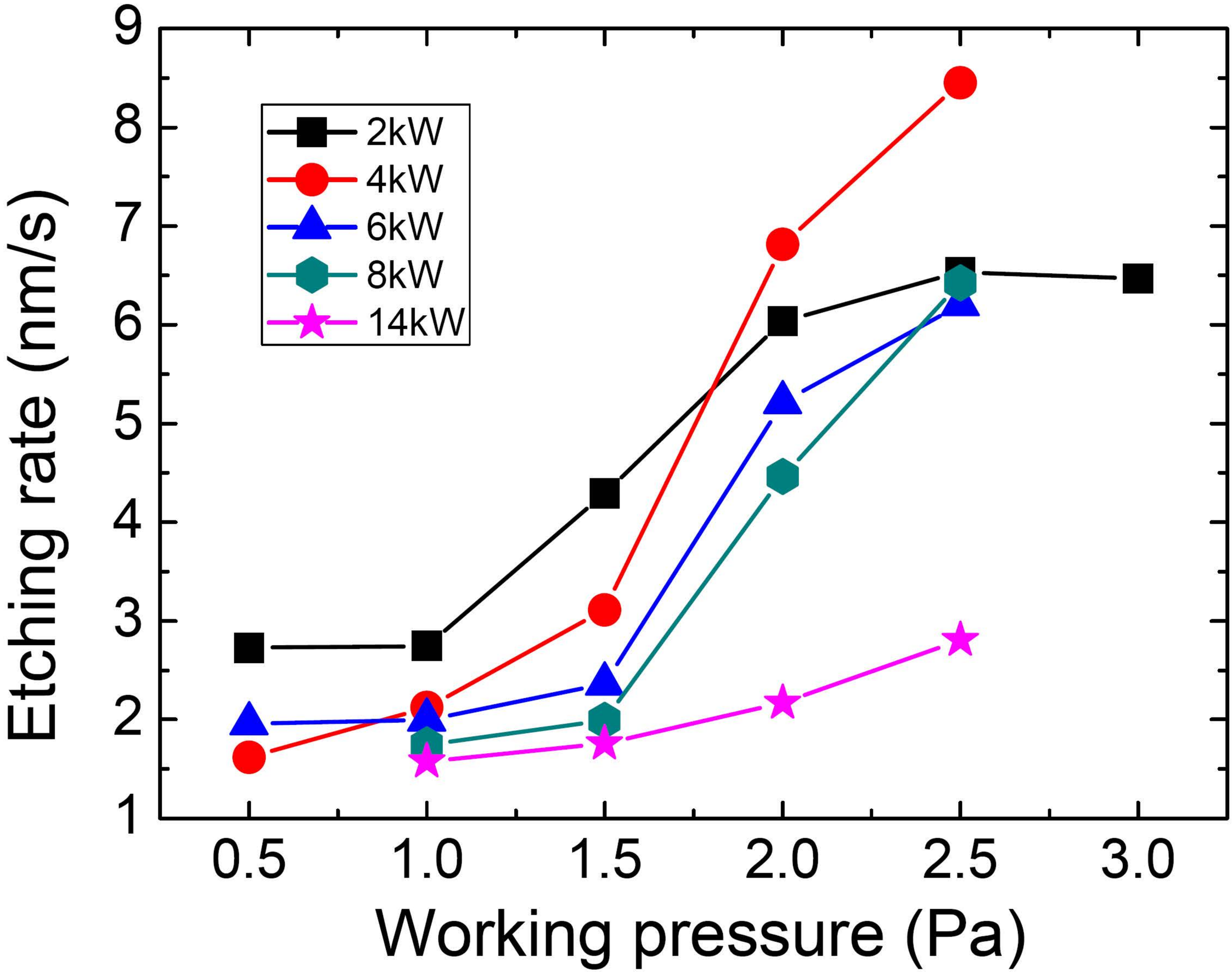
2kW
4kW
6kW
8kW
14kW
Etching rate (nm/s)
1
2
3
4
5
6
7
8
9
0.5
1.0
1.5
2.0
2.5
3.0
Working pressure (Pa)

Figure 11

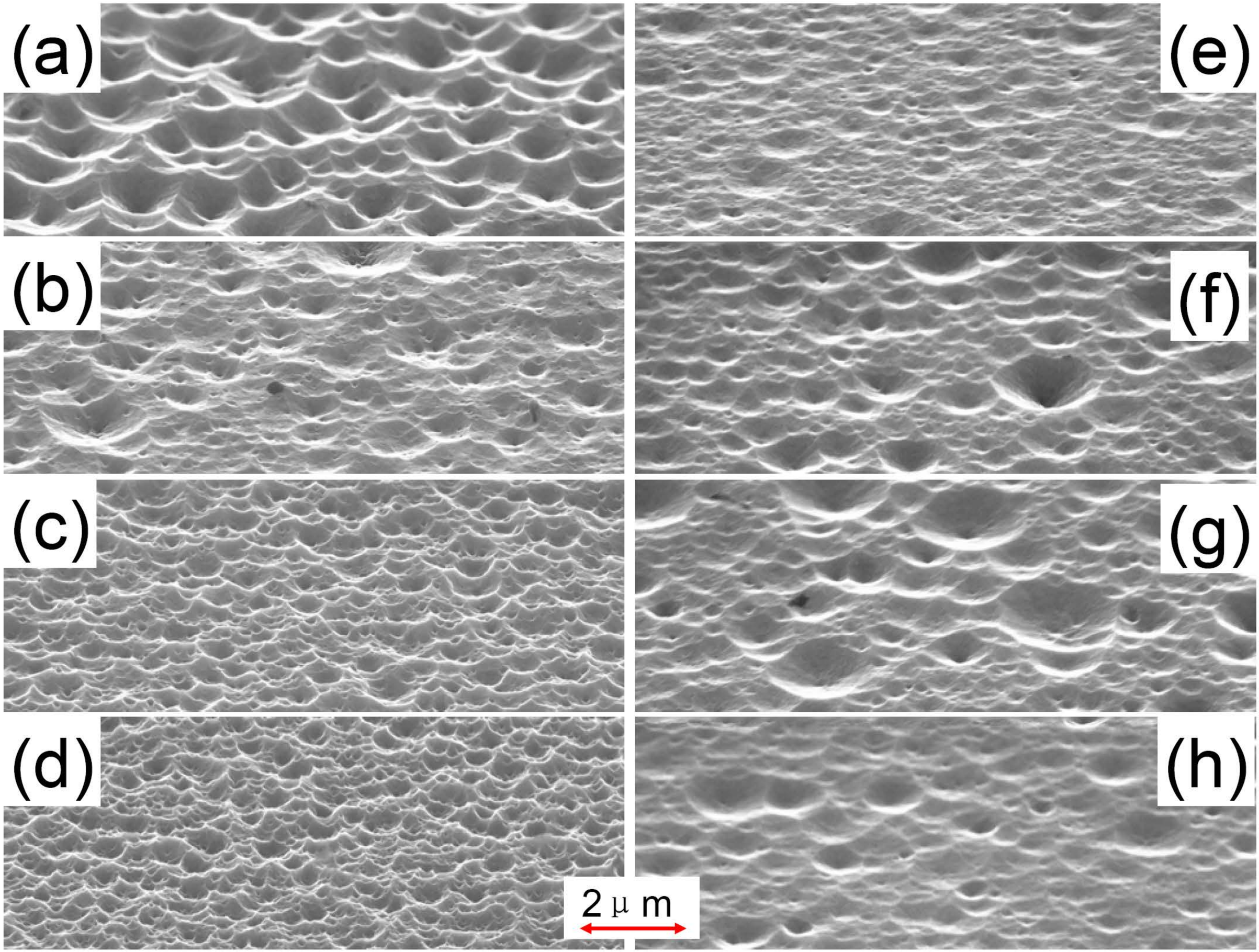

Figure 12

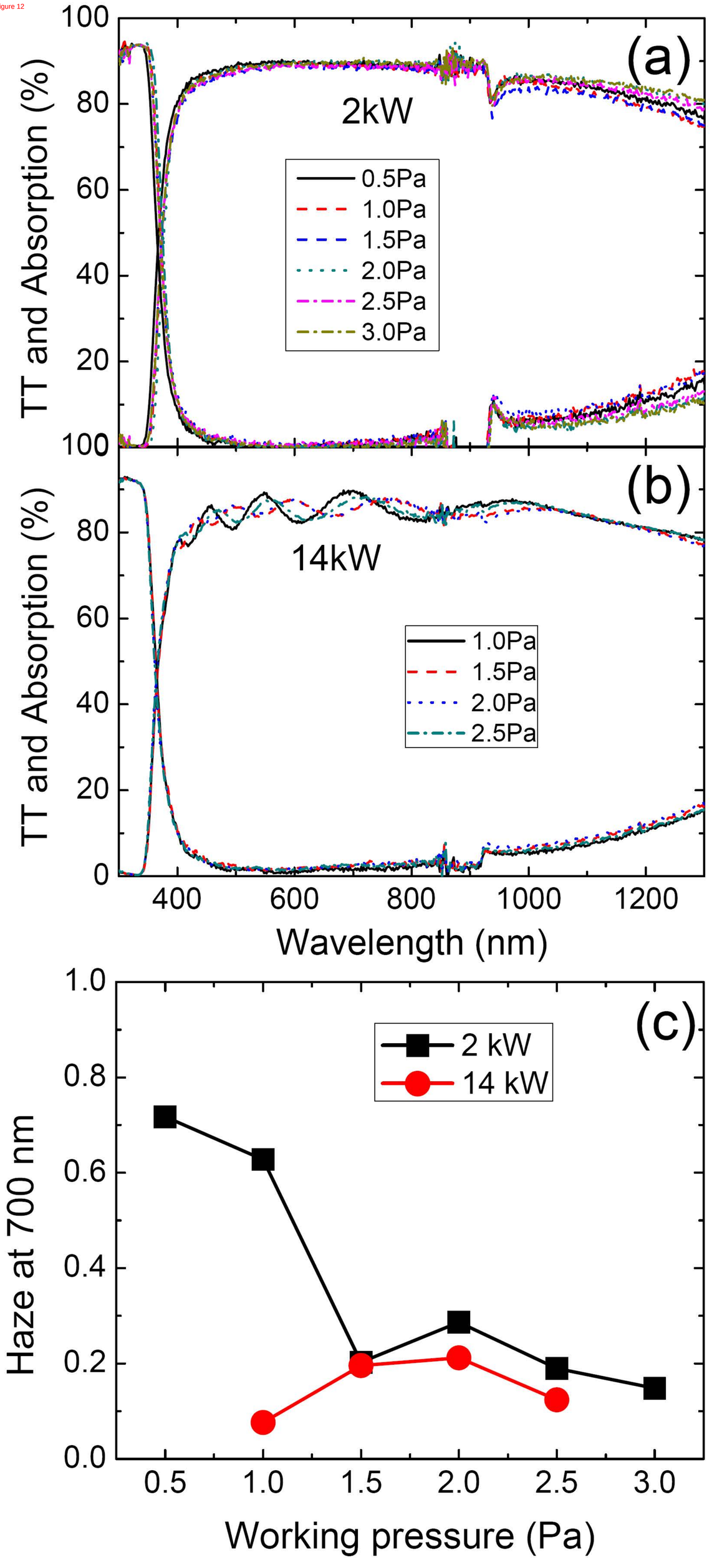
(a)
2kW
0.5Pa
1.0Pa
1.5Pa
2.0Pa
2.5Pa
3.0Pa
TT and Absorption (%)
(b)
14kW
1.0Pa
1.5Pa
2.0Pa
2.5Pa
TT and Absorption (%)
Wavelength (nm)
(c)
2 kW
14 kW
Haze at 700 nm
Working pressure (Pa)